Japanese Journal of Applied Physics

REGULAR PAPER

Populations and propagation behaviors of pure and mixed threading screw dislocations in physical vapor transport grown 4H-SiC crystals investigated using X-ray topography

To cite this article: Naoto Shinagawa *et al* 2020 *Jpn. J. Appl. Phys.* **59** 091002

Japanese Journal of Applied Physics **59**, 091002 (2020) **REGULAR PAPER**
https://doi.org/**10.35848/1347-4065/abab46**

Populations and propagation behaviors of pure and mixed threading screw dislocations in physical vapor transport grown 4H-SiC crystals investigated using X-ray topography

Naoto Shinagawa, Takuto Izawa, Morino Manabe, Tsuyoshi Yamochi, and Noboru Ohtani*

School of Science and Technology, Kwansei Gakuin University, 2-1 Gakuen, Sanda, Hyogo 669-1337, Japan

*E-mail: ohtani.noboru@kwansei.ac.jp

Received June 1, 2020; revised July 27, 2020; accepted July 31, 2020; published online August 20, 2020

The populations and propagation behaviors of pure and mixed threading screw dislocations (TSDs) in physical vapor transport (PVT) grown 4H-SiC crystals were investigated using X-ray topography. The X-ray topography studies revealed that mixed TSDs, which have a Burgers vector component within the basal plane in addition to the *c*-component, were dominant in PVT-grown 4H-SiC crystals, even though they have a higher energy contained in the elastic field around them compared to pure TSDs. The studies also revealed that mixed TSDs tended to propagate in a specific direction inclined from the *c*-axis, whereas pure TSDs were often converted into helical dislocations during the PVT growth. Based on these results, we discussed the nature and propagation behavior of pure and mixed TSDs in PVT-grown 4H-SiC crystals and suggested an importance of the interaction between TSDs and point defects during PVT growth of 4H-SiC.

1. Introduction

Over the last few decades, intensive effort has been devoted to the reduction of threading screw dislocations (TSDs) in 4H-SiC crystals grown by the physical vapor transport (PVT) growth method. TSDs often degrade the blocking capability of SiC power devices[1–3] and trigger the formation of epitaxial defects when crystals containing the dislocations are used as a substrate for SiC homoepitaxial growth.[4–7] According to Onda et al.,[8] TSDs in 4H-SiC are classified into four groups depending on their Burgers vectors. The first group is pure screw dislocations, i.e., threading pure screw dislocations denoted by TpSDs (Burgers vector: $\boldsymbol{c}$); the second group is threading mixed dislocations with a Burgers vector of $\langle 0001\rangle + \langle 1\bar{1}00\rangle$ (TMDs) (Burgers vector: $\boldsymbol{c} + \boldsymbol{m}$); the third group is threading screw dislocations having a Burgers vector of $\langle 0001\rangle + 1/3\langle 11\bar{2}0\rangle$ (TnSDs) (Burgers vector: $\boldsymbol{c} + \boldsymbol{a}$); and finally, the fourth group is threading screw dislocations having a Burgers vector with twice the magnitude of the *a*-component, $\langle 0001\rangle + 2/3\langle 11\bar{2}0\rangle$ (TM'D) (Burgers vector: $\boldsymbol{c} + 2\boldsymbol{a}$). They were reported to differently affect the device performance.[9] Onda et al. fabricated 4H-SiC *pin* diodes on a 4H-SiC epitaxial wafer containing these pure and mixed TSDs and found that one type of the mixed TSDs, i.e., TMDs, significantly degraded the blocking capabilities of the diodes, whereas another type of mixed TSDs, TnSDs, had almost no influence on the characteristics of the diodes even though the diodes were fabricated on the wafer areas containing TnSDs.[9]

Pure and mixed TSDs would also differently affect the device performance through the formation of epitaxial defects. TSDs often trigger the formation of crystallographic defects involving stacking faults in SiC epitaxial layers.[4–7] Benamara et al. reported that carrot defects, which are epitaxial defects having a serious impact on SiC devices, originated from TSDs existing in the substrate.[5] Carrot defects are defect complexes consisting of threading dislocations and prismatic and basal plane stacking faults, and these constituent defects have Burgers vectors or fault vectors of a mixed character, and thus, their characters and formation would be differently affected by pure and mixed TSDs when they are caused by TSDs in the substrate upon epitaxial growth. Pure and mixed TSDs also show different aspects when they are converted to Frank type stacking faults.[4,10] Tsuchida et al.[4] reported a conversion phenomenon of TSDs into Frank type stacking faults. They found a relatively simple array of $\boldsymbol{c}/4$ Frank partial dislocations in the epilayer, whereas Dudley et al. reported that more complicated stacking fault structures originated from TnSDs.[10]

These aspects of TSDs in 4H-SiC crystals described above make it crucial to fully classify pure and mixed TSDs in 4H-SiC crystals for discussing their influence on the device characteristics and achieving their reduction or eradication from SiC crystals. The determination of the Burgers vector of TSDs has been conducted using several characterization methods.[8,9,11–13] Sugawara et al.[11] determined the Burgers vector of a TSD using large-angle convergent-beam electron diffraction (LACBED) and revealed that the observed TSD, which was determined to be a TnSD by the LACBED analysis, did not dissociate into partial dislocations. Guo et al. determined the Burgers vector of TnSDs in 4H-SiC using synchrotron X-ray topography through the ray tracing simulation of the contrast patterns due to TnSDs.[12] Pure and mixed TSDs have also been studied by NaOH vapor etching. Yao et al.[13] conducted defect selective etching using NaOH vapor and found that TMDs caused a slightly different etch pit morphology compared to that due to TpSDs on the 4H-SiC (0001) surface. However, many aspects of pure and mixed TSDs are yet to be clarified. Particularly, the populations and propagation behaviors of pure and mixed TSDs in 4H-SiC crystals are not well understood. Understanding of these aspects is crucial for reducing the TSD density and improving the crystal quality of PVT-grown 4H-SiC crystals.

This paper deals with experimental investigation of the populations and propagation behaviors of pure and mixed TSDs in 4H-SiC crystals. Using a laboratory X-ray topography system, the Burgers vector analysis of pure and mixed TSDs in 4H-SiC crystals was conducted with various diffraction vectors, and the population of each type of TSD was determined by examining nearly 180 TSDs existing in 4H-SiC crystals. We also revealed characteristic propagation morphologies of pure and mixed TSDs depending on their Burgers vectors. Based on the obtained results, we discussed

the nature and propagation behavior of pure and mixed TSDs in PVT-grown 4H-SiC crystals.

2. Experimental methods

Approximately 65 mm diameter 4H-SiC single crystal boules were grown on an on-axis (000$\bar{1}$) 4H-SiC seed crystal by the PVT growth method. The typical growth temperature was about 2300 °C–2400 °C, and the inert (argon) gas pressure was maintained between 0.2–2.0 kPa during growth. The grown boules were nitrogen-doped and contained nitrogen donors in the mid-10^{18} cm^{-3} range. The grown boules were axially sliced into (11$\bar{2}$0) wafers (thickness: approximately 0.8 mm) for transmission X-ray topography.

Transmission X-ray topographs were taken from various portions of the axially sliced wafers with several symmetric and asymmetric diffractions using Mo $K_{\alpha 1}$ radiation. We used a commercial X-ray topography system (Lang projection topography) provided by Rigaku Corporation (XRT–100). The topographs were recorded using a charge-coupled device (CCD) camera with a pixel size of a few micrometers. A computer-controlled detection system took multiple several-millimeter-sized topographic images that were stitched together to form topographic images of a few centimeter size.

3. Results and discussion

3.1. Populations of pure and mixed TSDs in 4H-SiC crystals

Figure 1 shows schematic illustrations of (a) the PVT growth reactor of a 4H-SiC crystal and (b) the preparation scheme of a 4H-SiC (11$\bar{2}$0) wafer. The wafer was produced by axially slicing a 4H-SiC single crystal grown on a 4H-SiC (000$\bar{1}$)C seed crystal. In this study, we conducted X-ray topography for the upper portion of the wafer (well distant from the seed crystal) to investigate the nature and propagation behavior of pure and mixed TSDs in PVT-grown 4H-SiC crystals. To determine their Burgers vector, we took X-ray topographs with eight diffraction vectors, i.e., 000$\bar{8}$, $\bar{2}$110, $\bar{1}\bar{2}\bar{1}$0, $\bar{1}$100, $\bar{1}$101, $\bar{1}$10$\bar{1}$, 0$\bar{1}$11, and 0$\bar{1}\bar{1}$1. Table I summarizes the conditions of topographic contrast formation under various diffraction conditions based on the $\boldsymbol{g} \cdot \boldsymbol{b}$ analysis for the three types of TSDs, i.e., TMDs, TnSDs, and TpSDs, where the extinction conditions of the dislocation contrast are marked based on the invisibility criterion $\boldsymbol{g} \cdot \boldsymbol{b} = 0$. As shown in the table, with these eight diffraction vectors, the Burgers vector of twelve different types of mixed TSDs, i.e., TMDs and TnSDs, as well as one pure TSDs, i.e., TpSDs, are fully classified. In Table I, each Burgers vector shown in the table includes that of the opposite sign; for example, [1$\bar{1}$01] means both [1$\bar{1}$01] and [$\bar{1}$10$\bar{1}$]. The eight diffraction vectors were selected in terms of the diffraction intensity and the experimental availability of the incident and diffracted X-ray beams from the 4H-SiC (11$\bar{2}$0) wafer surface. PVT-grown 4H-SiC crystals are likely to also contain mixed TSDs with a multiple *a*- or *m*-component such as TM'D, as revealed by Onda et al.;[8] however, we assumed, based on the previous studies

Table I. Conditions of topographic contrast formation under various diffraction conditions for the three types of TSDs, i.e., TMDs, TnSDs, and TpSDs, based on the invisibility criterion $\boldsymbol{g} \cdot \boldsymbol{b} = 0$.

(✓ : extinction conditions of dislocation contrast)

		$\vec{b}$ \ $\vec{g}$	000$\bar{8}$	$\bar{2}$110	$\bar{1}\bar{2}\bar{1}$0	$\bar{1}$100	$\bar{1}$101	$\bar{1}$10$\bar{1}$	0$\bar{1}$11	0$\bar{1}\bar{1}$1
a	TMD	[1$\bar{1}$0$\bar{1}$]								
b		[1$\bar{1}$01]								✓
c		[10$\bar{1}\bar{1}$]			✓			✓		✓
d		[10$\bar{1}$1]			✓		✓		✓	
e		[0$\bar{1}\bar{1}$1]		✓				✓		
f		[0$\bar{1}$11]		✓			✓			
g	TnSD	1/3[1$\bar{2}$13]					✓			✓
h		1/3[1$\bar{2}\bar{1}\bar{3}$]						✓	✓	
i		1/3[2$\bar{1}\bar{1}$3]					✓			
j		1/3[2$\bar{1}$13]						✓		
k		1/3[11$\bar{2}$3]				✓			✓	
l		1/3[11$\bar{2}\bar{3}$]				✓				✓
m	TpSD	[0001]		✓	✓	✓				

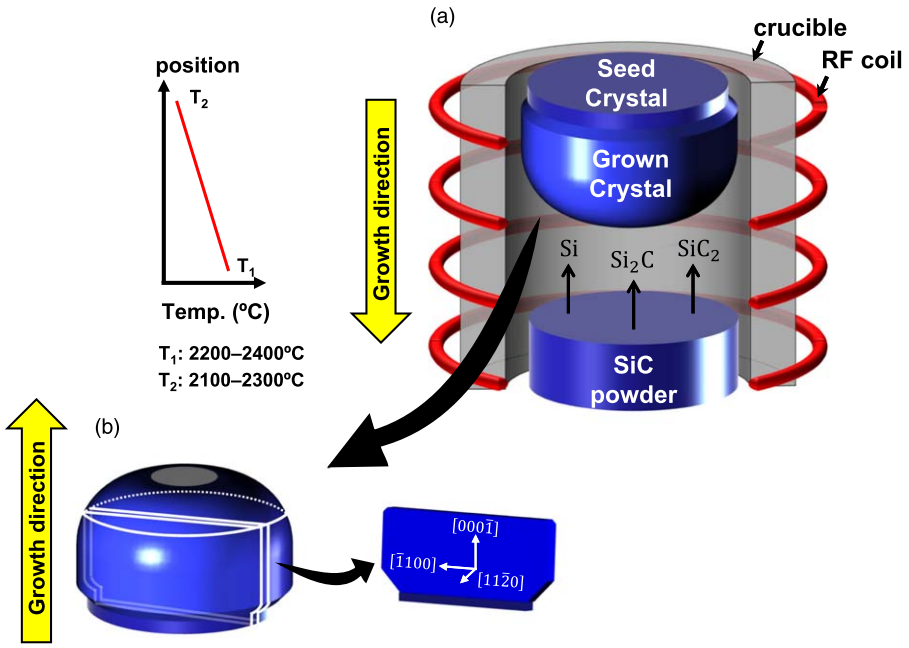

Fig. 1. (Color online) Schematic illustrations of (a) the PVT growth reactor of a 4H-SiC single crystal and (b) the preparation scheme of a 4H-SiC (11$\bar{2}$0) wafer. The wafer was produced by axially slicing a 4H-SiC crystal grown on a 4H-SiC (000$\bar{1}$)C seed crystal.

of TSDs in 4H-SiC crystals,[8–13] that they are minor in the crystals, and conducted X-ray topography analysis with a focus on the three types of TSDs, i.e., TMDs and TnSDs, and TpSDs in this study.

It should be noted here that owing to the fact that TSDs did not always propagate in the Burgers vector direction, diffraction contrasts caused by TSDs were not fully extinguished even when the invisibility criterion $\boldsymbol{g} \cdot \boldsymbol{b} = 0$ was satisfied. Hence, we concluded that the extinction condition was satisfied when the contrast was significantly reduced under the corresponding diffraction conditions compared to those under the other diffraction conditions shown in Table I. A similar consideration was also applied to threading edge dislocations (TEDs) existing in 4H-SiC crystals. They often propagate obliquely from the *c*-axis, and thus, they could have, in principle, weak diffraction contrasts even under the diffraction condition $\boldsymbol{g} = 000\bar{8}$. However, the diffraction contrasts due to TEDs are thought to be fairly weak compared to those caused by TSDs because of their relatively small Burgers vectors. In fact, in our X-ray topography experiments with $\boldsymbol{g} = 000\bar{8}$, TEDs were hardly imaged, and thus we have ascribed all the vertical line contrasts observed under $\boldsymbol{g} = 000\bar{8}$ to TSDs.

Figure 2 shows an example of the Burgers vector analysis of TSDs in a 4H-SiC crystal, where X-ray topographs with different diffraction vectors of the same portion of a 4H-SiC $(11\bar{2}0)$ wafer are shown. Figures 2(a)–2(d) show transmission X-ray topographs taken with $000\bar{8}$, $\bar{1}101$, $0\bar{1}1\bar{1}$, and $\bar{1}2\bar{1}0$ diffractions, respectively. In Fig. 2(a), six straight line contrasts are seen, which are indicated by open triangles and denoted by Roman numerals *i*, *ii*, *iii*, *iv*, *v*, and *vi*, respectively. Note that long slant lines occasionally observed in the topographs, at which the background contrast abruptly changes, corresponds to joint lines of stitched topographs. Figure 2(a) was taken with $000\bar{8}$ diffraction, and thus, all the observed straight line contrasts were caused by either type of TSDs, which have a Burgers vector component parallel to the *c*-axis. On the other hand, in Fig. 2(b) ($\boldsymbol{g} = \bar{1}101$) and Fig. 2(d) ($\boldsymbol{g} = \bar{1}2\bar{1}0$), TSD *v* is out of contrast, whereas TSD *vi* is out of contrast in Fig. 2(b) ($\boldsymbol{g} = \bar{1}101$) and Fig. 2(c) ($\boldsymbol{g} = 0\bar{1}1\bar{1}$). According to Table I, these results concluded that TSD *v* and TSD *vi* are a TMD with a Burgers vector of $[10\bar{1}1]$ and a TnSD with a Burgers vector of $1/3[1\bar{2}13]$, respectively. Similarly, based on additional X-ray topographs with other diffraction vectors, TSDs *i*, *ii*, *iii*, and *iv* were ascribed to TMDs with a Burgers vector of $[1\bar{1}0\bar{1}]$.

Another example is shown in Fig. 3, where X-ray topographs of another portion of the 4H-SiC $(11\bar{2}0)$ wafer are shown. Figures 3(a)–3(d) show transmission X-ray topographs taken with $000\bar{8}$, $\bar{1}101$, $\bar{2}110$, and $\bar{1}100$ diffractions, respectively. In Fig. 3(a), one wavy line contrast and two straight line contrasts are seen, which are indicated by open triangles and denoted by Roman numerals *vii*, *viii*, and *ix*, respectively. Figure 3(a) was taken with $000\bar{8}$ diffraction, and thus, all the wavy and straight line contrasts indicated by open triangles were caused by TSDs. On the other hand, in Fig. 3(c) ($\boldsymbol{g} = \bar{2}110$) and Fig. 3(d) ($\boldsymbol{g} = \bar{1}100$), wavy TSD *vii* is out of contrast, whereas TSDs *viii* and *ix* give rise to contrasts in all the topographs. Therefore, according to Table I, these results concluded that wavy TSD *vii* is a TpSD with a Burgers vector of [0001]. As to TSDs *viii* and *ix*, additional X-ray topographs with other diffraction vectors concluded that they are TnSDs with a Burgers vector of $1/3[1\bar{2}1\bar{3}]$.

We applied the same determination procedure of the Burgers vector of TSDs to a large portion of a 4H-SiC $(11\bar{2}0)$ wafer and determined the Burgers vectors of nearly 180 TSDs existing in the portion; X-ray topograph of the portion with the $000\bar{8}$ diffraction is shown in Fig. 4(a), whose location in the wafer is schematically illustrated in the left side of the topograph. Figure 4(b) shows the population of each type of TSD in that portion expressed by a pie chart, where "Undetermined" indicates the population of TSDs that exhibited topographic contrast patterns not belonging to those listed in Table I. As seen in the chart, major TSDs were TnSD and TMDs; both had similar populations but TnSDs were slightly more densely populated. It is noteworthy that TpSDs were minor in PVT-grown 4H-SiC crystals, even though they are accompanied by the smallest elastic energy around them. The minor population of TpSD was also reported by Onda et al. by examining TSDs in a 4H-SiC epitaxial layer using the LACBED technique.[8] They analyzed a total of 28 TSDs and observed TnSDs most frequently with a fraction of more than 50%, while only three out of 28 TSDs (10.7%) were found to be TpSDs.

In terms of the elastic energy, TpSDs are TSDs of the lowest energy; however, the population of TpSDs was quite low, implying that their population was determined by other

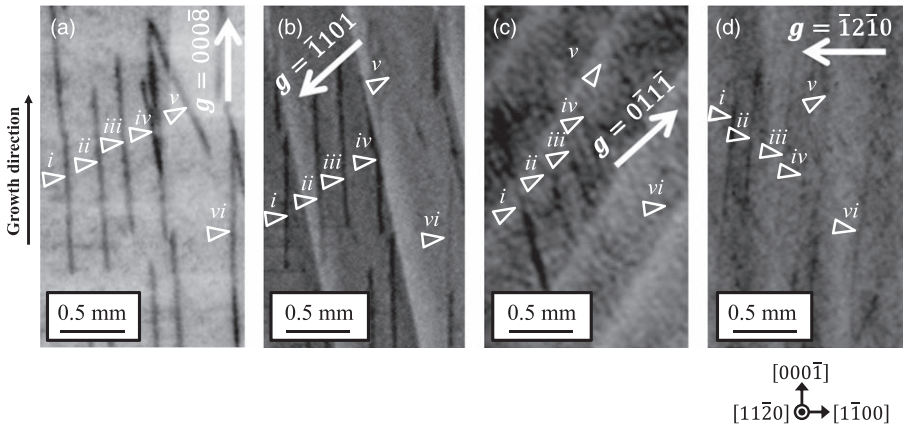

Fig. 2. Transmission X-ray topographs of an approximately 4.5 $mm^2 \times 0.8$ mm portion in an axially sliced 4H-SiC $(11\bar{2}0)$ wafer with (a) $000\bar{8}$, (b) $\bar{1}101$, (c) $0\bar{1}1\bar{1}$, and (d) $\bar{1}2\bar{1}0$ diffractions, where TSDs are indicated by open triangles.

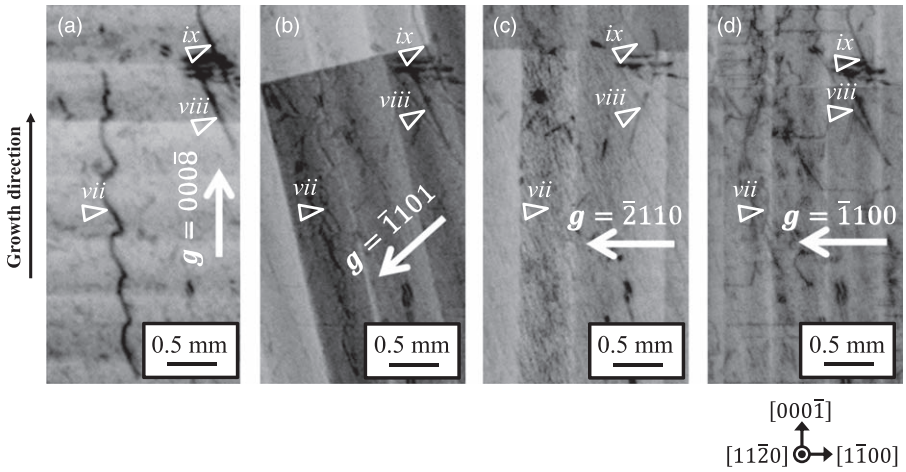

Fig. 3. Transmission X-ray topographs of another 7.5 $mm^2 \times 0.8$ mm portion in the axially sliced 4H-SiC $(11\bar{2}0)$ wafer with (a) $000\bar{8}$, (b) $\bar{1}101$, (c) $\bar{2}110$, and (d) $\bar{1}100$ diffractions, where TSDs are indicated by open triangles.

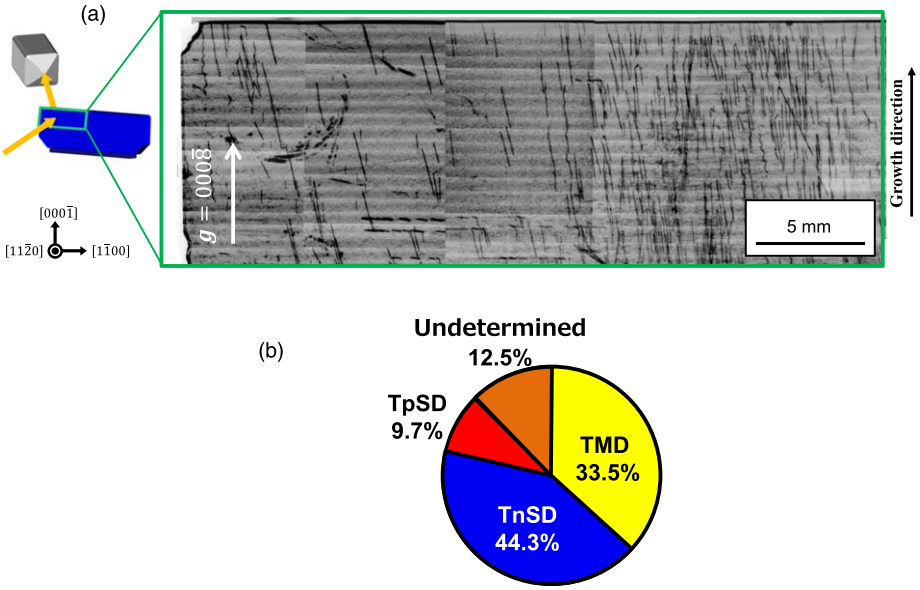

Fig. 4. (Color online) (a) Transmission X-ray topograph with the $000\bar{8}$ diffraction of a large portion in a 4H-SiC $(11\bar{2}0)$ wafer, whose location in the wafer is schematically illustrated in the left side of the topograph. (b) Population of each type of TSD in the portion, expressed by a pie chart.

factors. These factors are not clear at the moment but could be explained by considering the core energy of TSDs. The total dislocation energy per unit length is the sum of the energy contained in the elastic field around dislocation, E_{elas} and the energy in the dislocation core, E_{core}. The elastic energy E_{elas} is proportional to the square of the Burgers vector of dislocation, and thus, TpSDs, which have the shortest Burgers vector among pure and mixed TSDs, have the lowest elastic energy; however, if TpSDs have a larger core energy E_{core} than mixed TSDs, i.e., TnSDs and TMDs, TpSDs could have the largest total dislocation energy per unit length and show the smallest population in PVT-grown 4H-SiC crystals.

Another plausible mechanism has a kinematical origin. When TSDs are formed during PVT growth of 4H-SiC crystals, particularly at the initial stage of PVT growth, merger of dislocations having screw and edge components could happen. Several authors reported that most TSDs in PVT-grown 4H-SiC crystals were introduced into the crystals at the initial stage of the PVT growth,[14–20] whereas basal plane dislocation (BPD) networks were also reported to be formed at the grown crystal/seed crystal interface of PVT-grown 4H-SiC crystals.[21,22] The relationship between TSDs and BPD networks is still unclear but their interaction could result in TSDs having a Burgers vector component in the basal plane in addition to the *c*-component and control the populations of pure and mixed TSDs in PVT-grown 4H-SiC crystals.

3.2. Propagation behaviors of pure and mixed TSDs in 4H-SiC crystals

In the course of the determination process of the Burgers vectors of TSDs in PVT-grown 4H-SiC crystals, it was revealed that TSDs showed characteristic propagation morphologies in the crystals depending on their Burgers vectors. The first group is straight TSDs; examples are shown in Figs. 5(a) and 5(b), where X-ray topographs with the $000\bar{8}$ diffraction of two portions in a 4H-SiC $(11\bar{2}0)$ wafer are shown. In Fig. 5(a), three straight line contrasts due to TSDs are seen, as indicated by closed triangles in the figure. They are slightly inclined from the $[000\bar{1}]$ direction. Similarly, in Fig. 5(b), we observed ten straight line contrasts due to TSDs, as indicated by open triangles in the figure, and they

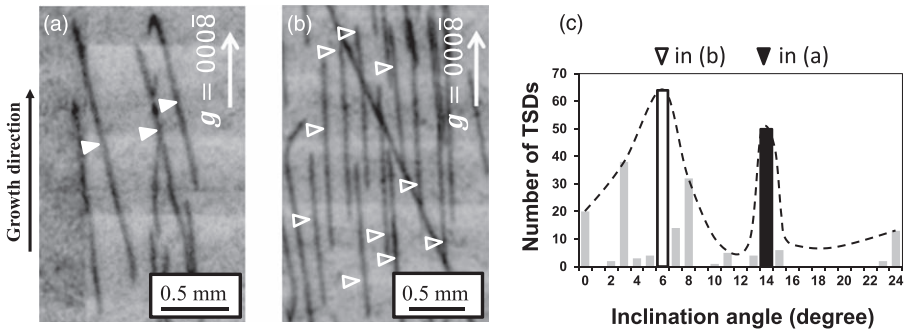

Fig. 5. X-ray topographs with the $000\bar{8}$ diffraction of two portions in a 4H-SiC $(11\bar{2}0)$ wafer, where straight line contrasts due to TSDs inclined (a) 14° and (b) 6° from $[000\bar{1}]$ are seen, as marked by closed and open triangles, respectively. (c) Histogram of the inclination angle from $[000\bar{1}]$ of TSDs exhibiting a straight line morphology in a 4H-SiC $(11\bar{2}0)$ wafer.

are also slightly inclined from $[000\bar{1}]$. An important feature to be noted here is that the inclined TSDs are all parallel to each other, implying that they would have a preferred inclination angle. It is well-know that TSDs tend to propagate in grown crystals perpendicularly to the growth front. This behavior was also observed in the crystals that we studied. As shown in Fig. 4(b), the crystal portion that we examined in Fig. 4(a) was located in the left side of the grown crystal. Therefore, most threading dislocations tended to be slightly inclined toward the left side of the crystal because of the dome-shaped growth front of the PVT-grown 4H-SiC crystal. However, close inspection of the propagation direction of straight TSDs in the crystal portion revealed that they were found to be inclined with a specific angle from the *c*-axis regardless of the growth front shape, which suggests that there could be a preferred propagation direction for TSDs.

A histogram of the inclination angle from $[000\bar{1}]$ of TSDs exhibiting a straight line morphology in a 4H-SiC $(11\bar{2}0)$ wafer is shown in Fig. 5(c). As seen in the figure, the histogram has two peaks around 6° and 14° from $[000\bar{1}]$; examples of TSDs with these inclination angles are shown in Figs. 5(b) and 5(a), respectively. It was found that TSDs with the inclination angle of 6° tended to be located in the central portion of the grown crystal, whereas those with the inclination angle of 14° were found both in the central and outer portions of the grown crystal. We examined the Burgers vector of these inclined straight TSDs and found that TSDs with the inclination angle of 6° from $[000\bar{1}]$ were mainly TMDs, and those inclined 14° were TnSDs. Particularly, most TnSDs propagating 14° from $[000\bar{1}]$ had a Burgers vector of $1/3[1\bar{2}13]$ or $1/3[1\bar{2}1\bar{3}]$.

The above-mentioned inclination angle is the projected angle onto the two-dimensional CCD camera and not the actual tilt angle of dislocations within the crystal. We estimated the actual tilt angle of TnSDs having a Burgers vector of $1/3[1\bar{2}13]$ or $1/3[1\bar{2}1\bar{3}]$ by assuming the TnSDs inclined from the *c*-axis toward the Burgers vector direction. The estimated tilt angle within the crystals was 26.5° from the *c*-axis but this angle did not coincide with the inclination angle of a specific crystal plane. Guo et al.[23] also investigated the line direction of a TnSD in a 4H-SiC (0001) wafer using synchrotron X-ray topography and found that the TnSD was slightly inclined (3.7°) from the *c*-axis but did not lie on a specific crystalline plane.

The inclination angle of threading dislocations in a 4H-SiC epilayer was discussed by Saka et al. in the framework of isotropic elastic theory of dislocations.[24] They calculated the inclination angles of TMDs and TnSDs having a minimum elastic energy in a 4H-SiC homoepitaxial layer grown on an off-oriented (4° or 8°) (0001) substrate toward $[11\bar{2}0]$. The obtained inclination angles were similar to those observed in this study. However, in their calculation, the epilayer thickness is a key parameter to determine the total elastic energy of threading dislocations in the epilayer. Therefore, their results cannot be straightforwardly applied to those described in this study, and thus, further investigation is needed to clarify the physical meaning of the inclined propagation of TSDs in 4H-SiC crystals.

The second group of TSDs showing a characteristic propagation morphology is wavy TSDs in PVT-grown 4H-SiC crystals, as exemplified by TSD *vii* shown in Fig. 3. Wavy TSDs were occasionally observed in 4H-SiC $(11\bar{2}0)$ wafers examined in this study, but their occurrence was relatively low (less than 5%). The $\boldsymbol{g} \cdot \boldsymbol{b}$ analysis was conducted on wavy TSDs and revealed that almost all the observed wavy TSDs were pure TSDs, TpSDs, whose Burgers vector is parallel to the *c*-axis, whereas non-wavy, fairly straight TpSDs were also observed. Based on these results, we concluded that wavy TSDs were helical dislocations formed during PVT growth of 4H-SiC crystals; originally straight TpSDs were converted to helical dislocations during PVT growth. As schematically illustrated in Fig. 6(a), in X-ray topography observations, helical dislocations are detected as wavy line contrasts on the CCD camera, and thus, the wavelength and amplitude of wavy line contrasts in X-ray topographs reflect the pitch and radius of helical dislocations in the crystals, respectively.

Similar wavy TSDs in PVT-grown 4H-SiC crystals were reported by Wu et al. using synchrotron X-ray topography.[25] They observed TSDs showing curved, slightly wavy morphologies in the crystals, and suggested that they were helical TSDs resulting from the interaction of a non-equilibrium concentration of vacancies with TSDs. They also found that the attractive interaction between closely located two helical TSDs with opposite signs of Burgers vectors resulted in partial annihilation of the dislocation lines.

In general, helical dislocations originate from screw dislocations, which can be converted into helical dislocations through a combined process of climb and glide motions of screw dislocations.[26] In this particular case of 4H-SiC, TpSDs climb perpendicularly to the *c*-axis by absorbing or emitting a certain type of intrinsic point defects, and

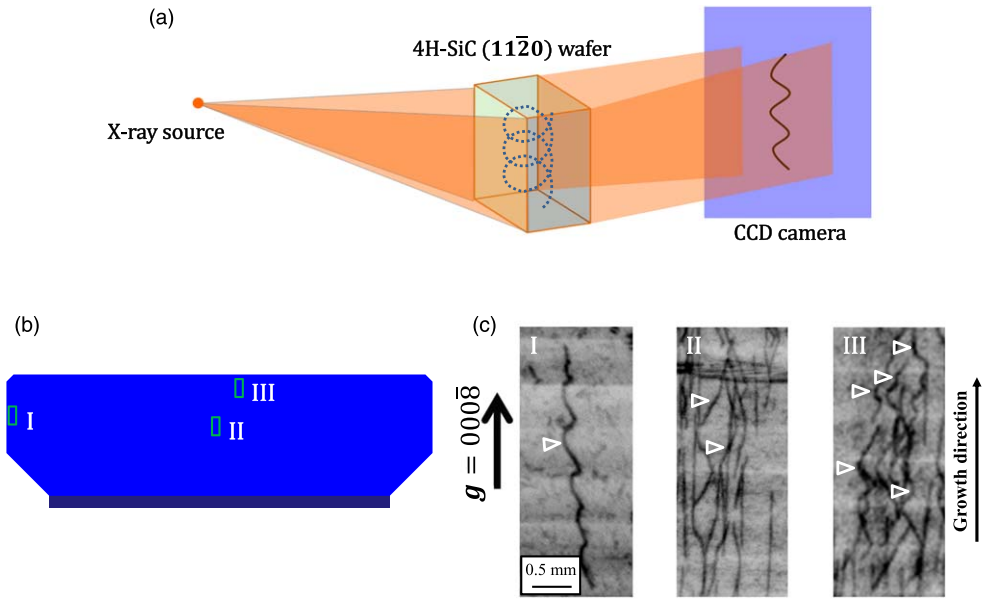

Fig. 6. (Color online) (a) Schematic illustration of X-ray topography observation of a helical dislocation, resulting in a wavy line contrast on the CCD camera. (c) Transmission X-ray topographs of helical TSDs showing various pitches and radii depending on the crystal portions where they existed. The locations of the crystal portions I, II, and III are schematically indicated in (b).

concurrently glide on the planes parallel to the *c*-axis. It is likely that the concurrent glide motion toward the Burgers vector direction more readily occurs in pure TSDs, and this would be the reason that almost all the observed wavy TSDs in this study were TpSDs.

With respect to the non-equilibrium concentration of point defects in PVT-grown 4H-SiC crystals, Shioura et al. recently demonstrated that a number of vacancies are injected into the growing crystal during PVT growth of 4H-SiC through the observation of the climb motion of BPD networks.[22] The formation of helical dislocations in SiC crystals would be another important indication of the vacancy injection into the growing crystal during PVT growth of 4H-SiC crystals. We examined a couple of portions in a 4H-SiC (11$\bar{2}$0) wafer and found several helical TpSDs. The locations of the portions that we examined in the wafer, denoted by Roman numerals I, II, and III, are schematically indicated in Fig. 6(b), and the helical TpSDs observed in X-ray topographs of the portions are shown in Fig. 6(c), where wavy TpSDs are marked by open triangles. As exemplified by the wavy TSD observed in crystal portion I, some helical TpSDs were found to propagate in the crystal in slightly inclined fashion toward the left side of the crystal (roughly perpendicularly to the growth front). Figure 6(c) clearly indicates that helical TpSDs showed different pitches and radii depending on the locations where they existed, and such variations in the shape of helical TpSDs would be indicative of the difference in the growth conditions of PVT growth process in terms of point defect (vacancy) injection. For example, the amplitude of wavy TSDs (radius of helical TSDs) would be a good indicator of the amount of vacancies injected into the growing crystal during PVT growth, which is a relevant parameter for controlling the PVT growth of 4H-SiC crystals.

4. Conclusions

We have investigated the populations and propagation behaviors of pure and mixed TSDs in PVT-grown 4H-SiC crystals using transmission X-ray topography. X-ray topography of (11$\bar{2}$0) wafers prepared by axially slicing nitrogen-doped PVT-grown 4H-SiC crystals revealed that mixed TSDs having a Burgers vector component within the basal plane in addition to the *c*-component were dominant in PVT-grown 4H-SiC crystals, whereas pure TSDs were minor. Mixed TSDs tended to exhibit a straight line morphology and were found to be inclined from the *c*-axis at a specific angle, suggesting that they would have a preferred propagation direction in the crystals. On the other hand, pure TSDs having a Burgers vector parallel to the *c*-axis exhibited a wavy propagation morphology in PVT-grown 4H-SiC crystals. The wavy morphology implies that pure TSDs in 4H-SiC crystals were converted into helical dislocations by absorbing or emitting point defects during PVT growth. On the basis of these results, we discussed the nature and propagation behavior of pure and mixed TSDs in PVT-grown 4H-SiC crystals.

ORCID iDs

Noboru Ohtani https://orcid.org/0000-0003-3678-7178

1) Q. Wahab, A. Ellison, A. Henry, E. Janzén, C. Hallin, J. Di Persio, and R. Martinez, Appl. Phys. Lett. **76**, 2725 (2000).
2) H. Fujiwara, H. Naruoka, M. Konishi, K. Hamada, T. Katsuno, T. Ishikawa, Y. Watanabe, and T. Endo, Appl. Phys. Lett. **100**, 242102 (2012).
3) K. Yamamoto, M. Nagaya, H. Watanabe, E. Okuno, T. Yamamoto, and S. Onda, Mater. Sci. Forum **717–720**, 477 (2012).
4) H. Tsuchida, I. Kamata, and M. Nagano, J. Cryst. Growth **310**, 757 (2008).
5) M. Benamara, X. Zhang, M. Skowronski, P. Ruterana, G. Nouet, J. J. Sumakeris, M. J. Paisley, and M. J. O'Loughlin, Appl. Phys. Lett. **86**, 021905 (2005).
6) J. Hassan, A. Henry, P. J. McNally, and J. P. Bergman, J. Cryst. Growth **313**, 1828 (2010).
7) T. Aigo, W. Ito, H. Tsuge, H. Yashiro, M. Katsuno, T. Fujimoto, and T. Yano, Mater. Sci. Forum **740–742**, 629 (2013).
8) S. Onda, H. Watanabe, T. I. Okamoto, H. Kondo, H. Uehigashi, and H. Saka, Phil. Mag. Lett. **95**, 489 (2015).

9) S. Onda, H. Watanabe, Y. Kito, H. Kondo, H. Uehigashi, N. Hosokawa, Y. Hisada, K. Shiraishi, and H. Saka, Phil. Mag. Lett. **93**, 439 (2013).
10) M. Dudley et al., Appl. Phys. Lett. **98**, 232110 (2011).
11) Y. Sugawara, M. Nakamori, Y. Z. Yao, Y. Ishikawa, K. Danno, H. Suzuki, T. Bessho, S. Yamaguchi, K. Nishikawa, and Y. Ikuhara, Appl. Phys. Express **5**, 081301 (2012).
12) J. Guo, Y. Yang, F. Wu, J. Sumakeris, R. T. Leonard, O. Goue, B. Raghothamachar, and M. Dudley, Mater. Sci. Forum **858**, 15 (2012).
13) Y. Z. Yao et al., Mater. Sci. Forum **858**, 389 (2016).
14) J. Takahashi, N. Ohtani, and M. Kanaya, J. Cryst. Growth **167**, 596 (1996).
15) E. K. Sanchez, J. Q. Liu, M. De Graef, M. Skowronski, W. M. Vetter, and M. Dudley, J. Appl. Phys. **91**, 1143 (2002).
16) A. R. Powell et al., Mater. Sci. Forum **457–460**, 41 (2004).
17) E. Tymicki, K. Grasza, R. Diduszko, R. Bożek, and M. Gała, Cryst. Res. Technol. **42**, 1232 (2007).
18) N. Ohtani, C. Ohshige, M. Katsuno, T. Fujimoto, S. Sato, H. Tsuge, W. Ohashi, T. Yano, H. Matsuhata, and M. Kitabatake, J. Cryst. Growth **386**, 9 (2014).
19) C. Ohshige, T. Takahashi, N. Ohtani, M. Katsuno, T. Fujimoto, S. Sato, H. Tsuge, T. Yano, H. Matsuhata, and M. Kitabatake, J. Cryst. Growth **408**, 1 (2014).
20) H. Suo, S. Tsukimoto, K. Eto, H. Osawa, T. Kato, and H. Okumura, Jpn. J. Appl. Phys. **57**, 065501 (2018).
21) K. Tani, T. Fujimoto, K. Kamei, K. Kusunoki, K. Seki, and T. Yano, Mater. Sci. Forum **858**, 73 (2016).
22) K. Shioura, N. Shinagawa, T. Izawa, and N. Ohtani, J. Cryst. Growth **515**, 58 (2019).
23) J. Guo, Y. Yang, F. Wu, J. Sumakeris, R. T. Leonard, O. Goue, B. Raghothamachar, and M. Dudley, J. Cryst. Growth **452**, 39 (2016).
24) H. Saka, H. Watanabe, Y. Kitou, H. Kondo, F. Hirose, and S. Onda, Jpn. J. Appl. Phys. **53**, 111302 (2014).
25) F. Wu, H. Wang, S. Byrapa, B. Raghothamachar, M. Dudley, E. K. Sanchez, D. Hansen, R. Drachev, S. G. Mueller, and M. J. Loboda, Mater. Sci. Forum **717–720**, 343 (2012).
26) D. Hull and D. J. Bacon, *Introduction to Dislocations* (Pergamon, Oxford, 1984) 3rd ed., p. 63.